Phantom Force Induced by Tunneling Current: A Characterization on Si(111)

A. J. Weymouth, T. Wutscher, J. Welker, T. Hofmann, and F. J. Giessibl
Institute of Experimental and Applied Physics, University of Regensburg, D-93053 Regensburg, Germany
(Received 8 March 2011; published 1 June 2011)

Simultaneous measurements of tunneling current and atomic forces provide complementary atomic-scale data of the electronic and structural properties of surfaces and adsorbates. With these data, we characterize a strong impact of the tunneling current on the measured force on samples with limited conductivity. The effect is a lowering of the effective gap voltage through sample resistance which in turn lowers the electrostatic attraction, resulting in an apparently repulsive force. This effect is expected to occur on other low-conductance samples, such as adsorbed molecules, and to strongly affect Kelvin probe measurements when tunneling occurs.

DOI: 10.1103/PhysRevLett.106.226801 PACS numbers: 73.63.Rt, 68.37.Ps, 73.50.−h

Scanning tunneling microscopy (STM) sparked enthusiasm in scanning probe microscopy with images of the adatoms of Si(111)-(7 × 7) [1]. Atomic force microscopy (AFM) removed the requirement for a conducting substrate [2] but brought more than just the possibility to measure on insulators [3]: Subatomic [4] and submolecular [5] imaging have also been demonstrated. These successes have brought strong interest in combined STM and AFM (e.g., [6,7]); however, the independence of force and current measurements remains an open issue [8–12].

Frequency-modulation AFM (FM-AFM) is a technique in which the interaction between tip and sample is measured by the frequency shift, Δf, of an oscillating tip from its eigenfrequency, f_0 [13]. Δf can be formulated as a measure of the force gradient, $k_{\mathrm{ts}} = -\frac{dF}{dz}$, where z is the distance from the surface. Δf is also a function of the spring constant of the oscillator, k, the amplitude of oscillation, A, and z, and can be approximated at small amplitudes by $\Delta f \approx (f_0/2k)k_{\mathrm{ts}}$ [14]. In short, a decrease in Δf indicates that the force between the tip and sample is becoming more attractive.

In contrast to the tunneling current, I, measured with STM, Δf is not monotonic as a function of z. The local tip-sample interaction is usually well represented by a Morse potential from which the force and the force gradient can be derived, as shown in Fig. 1(a). In region I, k_{ts} decreases as z decreases. Long-range forces (e.g., van der Waals) cause attractive interaction between tip and sample. It is in this region STM is usually conducted on Si(111)-(7 × 7), at setpoints under 10 nA at 1 V, corresponding to tip-sample distances greater than 5 Å [15]. In region II, k_{ts} increases as z decreases. The waveform overlap between tip and sample causes measurable energy increase due to Pauli repulsion, which states electrons may not occupy the same quantum state [16].

In this Letter, we report upon the effect of bias voltage on FM-AFM of Si(111)-(7 × 7). At tip-sample distances corresponding to normal STM setpoints, one expects a decrease in frequency shift as the tip moves laterally without feedback over an adatom, due to the increase in attractive force [17]. However, with the application of a moderate bias voltage (> 1.0 V), one is able to observe a frequency shift increase as the tip moves over an adatom. Moreover, FM-AFM images taken with this applied bias voltage can show atomic contrast at tip-sample distances 300 pm, further from the surface than is required to image with no applied bias. We propose a model incorporating sample resistance where the observed frequency shift is

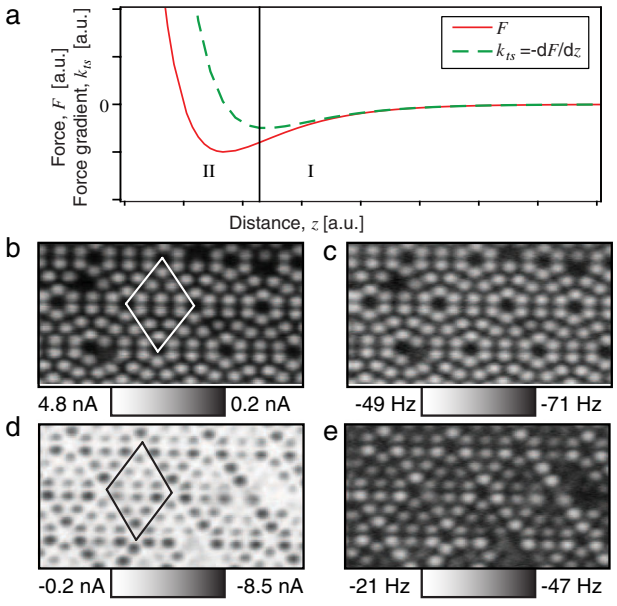

FIG. 1 (color online). (a) From a Morse potential, the force and force gradient can be calculated. At $V_{\mathrm{tip}} = -1.5$ V, (b) current and (c) force data are collected without I or Δf feedback. Similar data are shown at $V_{\mathrm{tip}} = +1.5$ V; the (d) current data appears inverted because in opposite bias voltages, current flow is reversed, however (e) Δf again increases above the adatoms. Data were collected at $A = 400$ pm, $f_0 = 25\,908$ Hz. In STM data, a unit cell of 7 × 7 is highlighted; images are 10 nm × 5.5 nm.

caused by a decrease in the electrostatic attraction between tip and sample.

Experiments were performed with a qPlus sensor with $k = 1800\ \mathrm{N\,m^{-1}}$ and W tips. Data were collected in constant height mode with both a home-built microscope operating at room temperature in UHV and, where explicitly stated, at 4.5 K with an Omicron LT-SPM wired similar to [18]. Reported current I is an averaged current and biases refer to the tip with respect to the sample. Two types of p-doped Si(111) samples were used: a high-doped sample corresponding to a resistivity $\rho = 0.010$–$0.012\ \Omega\,\mathrm{cm}$ at 300 K and a low-doped sample with $\rho = 6$–$9\ \Omega\,\mathrm{cm}$ at 300 K. Si(111)-(7×7) was prepared with several flash and anneal cycles.

Figures 1(b)–1(e) show simultaneously acquired I and Δf data of the low-doped Si(111) sample. In (b) and (c), the bias was $V_{\mathrm{tip}} = -1.5$ V. STM data show the clear structure of the 7×7 reconstruction, with all adatoms in the unit cell having approximately the same intensity. The Δf data show an increase in frequency shift above the adatoms. In (d) and (e), the bias was $V_{\mathrm{tip}} = +1.5$ V. The STM data show different features in the outlined unit cell: over adatoms in the faulted half (the lower six adatoms), we record greater absolute current than over those in the unfaulted half, as expected [19]. The Δf data, however, also have stronger contrast above the faulted half unit cell. In a simple picture of AFM in which the total electron density is measured [20], one would not expect this Δf contrast to depend upon bias voltage. Also, while one might initially propose that this increase in Δf over adatoms indicates that we are in region II of the Morse potential, we show later (with respect to the data in Fig. 3) that this is not the case.

The relation between Δf and I channels can be further characterized. For each pixel in the images in Figs. 1(b)–1(e), Δf and I data have been acquired. Before a pixel-by-pixel comparison of I and Δf can be made, however, the low bandwidth phase locked loop (PLL) used to measure Δf must be taken into account. At scan speeds as low as $20\ \mathrm{nm\,s^{-1}}$, it can cause a noticeable lateral displacement between Δf and I data. Consider a scan line 10 nm long with 256 pixels. The bandwidth of our PLL is 120 Hz. Assuming the I data to be instantaneous, the Δf data are offset by $(256\ \mathrm{pixels}/10\ \mathrm{nm}) \times 20\ \mathrm{nm\,s^{-1}}/120\ \mathrm{Hz} \approx 4$ pixels. Independently, a cross correlation of Figs. 1(b) and 1(c) shows a 4 pixel offset.

Each measurement of I thus has an associated Δf measurement, as is shown in Fig. 2(a). The fact that there is some correspondence is not surprising, as regularly, force and current images of the same surface appear similar. What is surprising is that the data are quite linear and Δf increases over the entire current range.

The slope of the linear fit to the data in Fig. 2(a) is a measure of the Δf response as a function of I. This analysis was repeated with images at various biases.

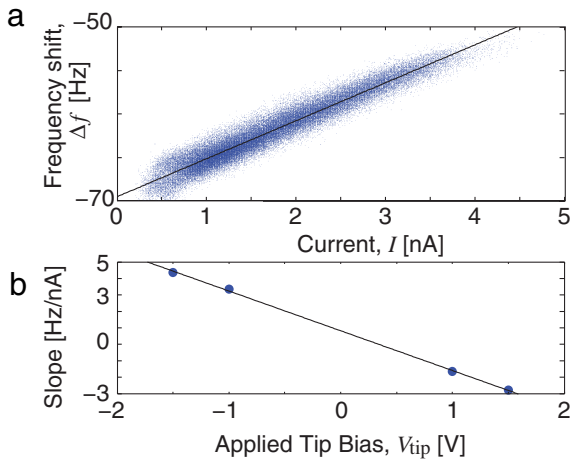

FIG. 2 (color online). (a) From Figs. 1(b) and 1(c), a comparison between I and Δf can be made. Their relationship is linear; the line shown has a slope of 4.36 Hz/nA. (b) Following similar analyses at other biases ($V_{\mathrm{tip}} = -1.5$, -1.0, 1.0 and 1.5 V) the slopes of the fits can be plotted as a function of the bias. I has the opposite sign as V_{tip}. A linear fit is shown as a guide to the eye.

Figure 2(b) shows the slopes of these fits with respect to bias. The observation is that not only does this repulsive Δf signal scale linearly with current, but that this $\Delta f/I$ slope itself scales with applied bias voltage.

We then performed measurements with the high-doped sample. At room temperature, this apparently repulsive Δf contrast was not observable in the current range of $|I| < 5$ nA. At 4.5 K, however, it was, as shown in Fig. 3(a): In cooling the system, the effective resistance increased and this Δf contrast was again easily observed.

In order to investigate the tip-sample distance, the bias was reduced to zero partway through image acquisition. The result is shown in Fig. 3(b). In this case, the contrast in Δf disappears with the lack of an applied bias voltage. Atomic contrast in Δf should be observable without an

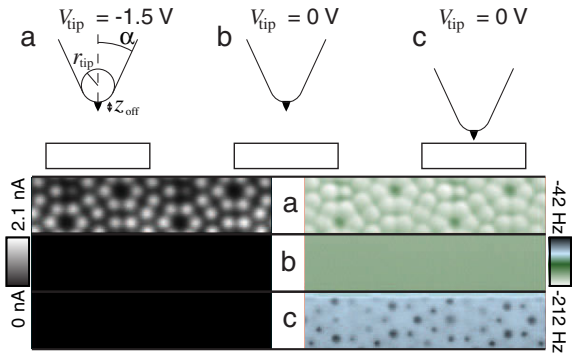

FIG. 3 (color online). Top: Schematic of the experiment. Bottom: Simultaneous I and Δf data acquired at 4.5 K. (a) $V_{\mathrm{tip}} = -1.5$ V.(b) $V_{\mathrm{tip}} = 0$ V.(c) Tip is approached 340 pm closer to the surface. Data were collected at $A = 100$ pm, $f_0 = 16777$ Hz, and images are 8 nm × 8 nm.

applied bias voltage [21]. In order to observe Δf contrast with no applied bias voltage, we needed to advance the tip 340 pm closer to the surface. The remainder of the image, in Fig. 3(c), clearly shows the expected contrast in Δf.

One might ask what effect removal of the bias voltage has upon the average tip-sample distance, knowing that there is an electrostatic force between tip and sample that scales as the square of the voltage difference [22]. We have found, in agreement with previous studies [23], that to describe long-range electrostatic interaction between the tip and sample, a model of the tip consisting of a rounded cone and a small nanotip, as shown in Fig. 3(a), is quite accurate. The rounded cone accounts for the electrostatic interaction and the nanotip performs the imaging. Typical values to describe our tips are $r_{\text{tip}} = 5$ nm, $\alpha = 70°$, and $z_{\text{off}} = 1$ nm, resulting in an average force, over one oscillation, of 30 nN when $V_{\text{tip}} = 2$ V. Following [20], the effect of removing this bias is that the average tip-sample distance would increase by only 17 pm. Thus, even accounting for the effect of removing the bias voltage, we needed to approach the tip by more than 300 pm towards the surface to observe the Δf contrast in Fig. 3(c). It is therefore not possible that the frequency shift increase [e.g., in Fig. 1 or Fig. 3(a)] was recorded in region I where Pauli repulsion dominates.

We now consider the effect of the sample having a resistance given by R_s, with the tip biased at V_{tip}. The electrostatic interaction between tip and sample causes a force that scales as the square of the voltage difference, $(V_{\text{tip}} - V_{\text{sample}})^2$. We neglect the contact potential difference, V_{cpd}, because it is simply an offset of the applied bias voltage. This is highly tip dependant and is typically in the range of 0.4 ± 0.3 V; we propose that this could account for the asymmetry in Fig. 2(b). While local variations in V_{cpd} have been reported on the 7×7 surface with Kelvin probe measurements [24], they would not lead to an increase in Δf over adatoms in both bias polarities. Letting K represent the prefactor which is independent of bias [22]:

$$F^{\text{es}} = -K(V_{\text{tip}}^2 - 2V_{\text{tip}}IR_s + I^2R_s^2). \quad (1)$$

Assuming $V_{\text{sample}} = IR_s \ll V_{\text{tip}}$, the second order term can be discarded. Proceeding with the derivative to k_{ts}, where $I = I_0 \exp(-\kappa z)$:

$$k_{\text{ts}}^{\text{es}} \equiv -\frac{dF^{\text{es}}}{dz} = \frac{dK}{dz}V_{\text{tip}}^2 - \left(2\frac{dK}{dz} - 2K\kappa\right)V_{\text{tip}}R_sI. \quad (2)$$

Δf is, in the small amplitude approximation, directly proportional to k_{ts}, and if $k_{\text{ts}}^{\text{es}}$ is dominant, Δf would have a linear response with respect to I and a slope that is linearly proportional to V_{tip}.

To test this theory, we performed an experiment shown schematically in the top third of Fig. 4. A switch was installed between the high-doped sample and the virtual ground. The virtual ground is provided by the operational amplifier used to detect the tunneling current. The switch is used to add known resistances $R_1 = 10$ MΩ and $R_2 = 30$ MΩ. Δf should now follow the relation:

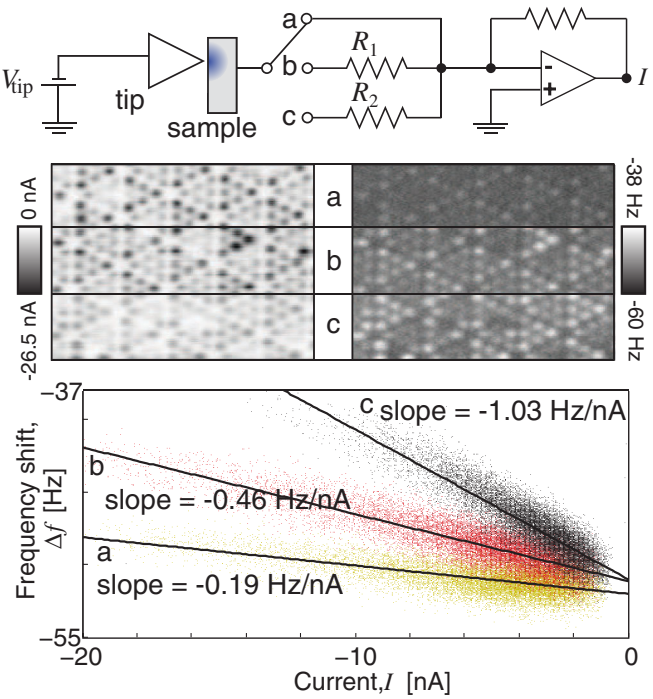

FIG. 4 (color online). Top: Schematic of the experiment. Middle: Simultaneous I and Δf data. Bottom: Δf versus I data. (a) $R = 0$ between sample and ground. (b) $R_1 = 10$ MΩ (c) $R_2 = 30$ MΩ. See text for details. Data were acquired with $V_{\text{tip}} = 1.5$ V, $A = 400$ pm, $f_0 = 19390$ Hz and are 10 nm × 7 nm.

$$\Delta f = b + mV_{\text{tip}}(R_s + R)I \quad (3)$$

where R is either 0, R_1 or R_2, depending on the switch, m is independent of R_s, V_{tip} and I, and b is independent of I. Considering the I-dependent term in Eq. (3), m and R_s are unknown. The data collected at $R = 0$ and $R = R_1$ can be used to determine m and R_s, and then to predict a slope of -0.99 Hz/nA when $R = R_2$. The data and the slopes for the three switch settings are shown in Fig. 4; the observed slope when $R = R_2$ is -1.03 Hz/nA.

This strong agreement with our simple model, incorporating a sample resistance R_s, prompts us to further explain the mechanism of this model. Our fit parameters, for example, indicate that for the low-doped sample $R_s =$ 164 MΩ. While this number seems high, the tunneling current is injected in a very small area, and this in effect creates a large current density that must disperse through a relatively small area. Assuming that the current I is injected in an area of radius 1 Å, and then disperses through the sample radially, we can use classical electrodynamics to determine the order of magnitude of the expected resistance. The current density then scales as $1/(2\pi r^2)$, where r is the distance from the current injection, and is directly

proportional to the derivative of the electrochemical potential via the sample resistivity. The voltage difference between the area in which the tunnel current is injected and a position in the bulk sufficiently far away is thus

$$V_{\text{sample}} = R_s I = \frac{\rho}{2\pi(1\ \text{Å})} I. \quad (4)$$

Given this sample has a resistivity $\rho = 6$ to 9 Ω cm, R_s is in the range of 96 to 143 MΩ, which agrees well with the fitted R_s value. In this simple picture, the voltage drop would be highly local, but the charge density and electric field are both most intense near the tip apex, where one would expect the highest contribution to the electrostatic attraction. This picture also has a much higher error when we consider the high-doped sample, and it is likely that an atomic-scale theory of electronic conductance is required to fully explain the observed R_s. Finally, it should be noted that tip induced band bending does not play a strong role on the 7×7 surface (e.g., tunneling spectra agree well with photoemission data as in [19]) but that charging near the tip-sample junction can lead to a modified tunneling spectrum [26].

To summarize, we observe a frequency shift increase over adatoms that scales linearly with current.

As far back as simultaneous FM-AFM and STM have been attempted, contrast inversion has been observed as a function of tip state and of applied bias voltage [8–10]. Guggisberg and co-workers suggest that short-range electrostatics might explain the contrast inversion, but do not propose a model for this [11]. Contrast inversion can be explained within our model quite easily: At low biases, the tip images the adatoms as predicted by theory, and shows a negative Δf contrast over adatoms, while at higher biases, the Δf contrast is due primarily to the decrease in capacitive attraction due to the sample resistance and tunnel current, as reported in this Letter.

High spatial resolution demands short-range forces, which implies small tip-sample distances. With simultaneous AFM and STM, one must be aware that a moderate tip-sample bias can also produce a tunnel current so large that it would affect the surface potential and measurable Δf contrast. On thin metal layers at low voltages [25] and metal surfaces [6], this effect is ignorable. For example, Cu has a $\rho \approx 2 \times 10^{-8}$ Ωm; even at $V_{\text{tip}} = 10$ V and $I = 100$ nA, the expected Δf would be <1 mHz. However this effect must be taken account of when performing combined STM and AFM of any surface with appreciable resistivity, including, of course, semiconductor surfaces.

We thank J. Repp, M. Emmrich, and M. Schneiderbauer for discussions, and J. Mannhart and the DFG (SFB 689) for support.

[1] G. Binnig *et al.*, Phys. Rev. Lett. **50**, 120 (1983).
[2] G. Binnig, C. F. Quate, and C. Gerber, Phys. Rev. Lett. **56**, 930 (1986).
[3] F. J. Giessibl and G. Binnig, Ultramicroscopy **42–44**, 281 (1992).
[4] F. J. Giessibl *et al.*, Science **289**, 422 (2000).
[5] L. Gross *et al.*, Science **325**, 1110 (2009).
[6] M. Ternes *et al.*, Phys. Rev. Lett. **106**, 016802 (2011).
[7] W. A. Hofer and A. J. Fisher, Phys. Rev. Lett. **91**, 036803 (2003).
[8] S. Molitor, P. Güthner, and T. Berghaus, Appl. Surf. Sci. **140**, 276 (1999).
[9] T. Arai and M. Tomitori, Jpn. J. Appl. Phys. **39**, 3753 (2000).
[10] T. Arai and M. Tomitori, Appl. Surf. Sci. **157**, 207 (2000).
[11] M. Guggisberg *et al.*, Appl. Phys. A **72**, S19 (2001).
[12] Y. Sugimoto *et al.*, Phys. Rev. B **81**, 245322 (2010).
[13] T. Albrecht *et al.*, J. Appl. Phys. **69**, 668 (1991).
[14] F. J. Giessibl, Appl. Phys. Lett. **78**, 123 (2001).
[15] P. Jelínek *et al.*, Phys. Rev. Lett. **101**, 176101 (2008).
[16] N. Moll *et al.*, New J. Phys. **12**, 125020 (2010).
[17] R. Pérez *et al.*, Phys. Rev. Lett. **78**, 678 (1997).
[18] F. J. Giessibl, Appl. Phys. Lett. **76**, 1470 (2000).
[19] R. J. Hamers, R. M. Tromp, and J. E. Demuth, Phys. Rev. Lett. **56**, 1972 (1986).
[20] S. Hembacher, F. J. Giessibl, and J. Mannhart, Science **305**, 380 (2004).
[21] F. J. Giessibl, Science **267**, 68 (1995).
[22] S. Hudlet *et al.*, Eur. Phys. J. B **2**, 5 (1998).
[23] M. Guggisberg *et al.*, Phys. Rev. B **61**, 11151 (2000).
[24] S. Sadewasser *et al.*, Phys. Rev. Lett. **103**, 266103 (2009).
[25] Y. Sun *et al.*, Phys. Rev. B **71**, 193407 (2005).
[26] R. M. Feenstra, G. Meyer, and K. H. Rieder, Phys. Rev. B **69**, 081309(R) (2004).